Numerical analysis of the mitigation of aerodynamic loads in low-rise buildings using spoilers with PID control

Gabriela P. Bianchin[1], Alexandre L. Braun[1]

[1]*Programa de Pós-Graduação em Engenharia Civil (PPGEC), Universidade Federal do Rio Grande do Sul (UFRGS)*
Av. Osvaldo Aranha, 99, 90035-190, Porto Alegre/Rio Grande do Sul, Brasil
gabriela_bianchin@hotmail.com, alexandre.braun@ufrgs.br

Abstract. A numerical investigation is performed in this work to evaluate the influence of controlled spoilers on pressure mitigation over low-rise building roofs. Considering that low-rise buildings are susceptible to severe damages caused by wind action, spoilers are utilized along the roof windward edges to reduce the aerodynamic load, which are controlled using PID control techniques. Numerical simulations are carried out using a semi-implicit CBS algorithm, where linear tetrahedral finite elements are employed for spatial discretization in a standard Galerkin procedure. Turbulence modeling is performed using Large Eddy Simulation and the flow fundamental equations are written considering isothermal and incompressible conditions in arbitrary Lagrangian-Eulerian kinematical description to take into account the spoiler angular motion. Two and three-dimensional simulations are carried out using a typical low-rise building model, where the influence of controlled roof spoilers and wall openings on the roof loading is evaluated. Wind tunnel predictions are utilized to validate the numerical formulation proposed here.

Keywords: Low-rise buildings, Pressure mitigation, PID control, Large Eddy Simulation (LES), Finite Element Method (FEM).

1 Introduction

Low-rise buildings subject to wind action develop strong vortices on the roof surfaces, specifically at the transition between wall and roof, which generate high suction peaks in these regions. When openings are located on the windward wall, large positive pressures are transmitted to the internal environment of the building and a combination between external and internal pressures may result in intense lift loads applied to the roof structure. In this sense, Li et al. [1] investigated the wind pressure mitigation effect on the roof of a low-rise gable-roof building with spoilers using wind tunnel experiments. The experimental predictions showed the maximum pressure mitigation is obtained when spoilers are located at the gable, followed by spoilers located at the eave.

Control surfaces have been adopted to suppress aeroelastic instabilities and reduce aerodynamic loads due to wind action on tall buildings and long-span bridges (see, for instance, Sangalli and Braun [2]). These aerodynamic appendices can also be designed to reduce the wind loading on low-rise building roofs, which may be automatically adjusted according to instantaneous flow conditions. In this sense, PID control techniques could be employed to determine the orientation of spoilers (see for details on PID controllers in Aström and Hägglund [3] and Aström and Hägglund [4]).

In the present work, the influence of controlled spoilers on the wind load over the roof surface is evaluated considering building models with and without openings in the lateral walls. A finite element model based on the semi-implicit CBS scheme is utilized, where linear tetrahedral elements are adopted for spatial discretization. The flow fundamental equations are written using an Arbitrary Lagrangian-Eulerian (ALE) kinematical description, where Large Eddy Simulation (LES) is adopted for turbulence modeling, and a mesh motion scheme is employed to accommodate spoiler motions within the flow spatial field. Two-dimensional preliminary simulations are

performed considering a typical low-rise building model in order to calibrate the control formulation for spoilers located at the roof windward edge, where the influence of wall openings on the roof loading is also considered. The numerical formulation proposed here is validated using three-dimensional simulations based on wind tunnel tests referring to a typical low-rise building model.

2 Equations

2.1 Flow considerations

Some physical assumptions concerning the fluid flow modeling adopted here are initially presented (see, for instance, Braun and Awruch [5]): natural wind streams are considered to be within the incompressible and turbulent flow range; wind is constantly flowing with a constant temperature (isothermal process); gravity forces are neglected in the flow field; air is considered mechanically as a Newtonian fluid.

Consequently, the flow fundamental equations are reduced to the well-known Navier-Stokes and continuity equations, which are written here using an ALE kinematical description to consider the presence of moving bodies immersed in the flow field, while the flow turbulence is resolved using LES and Smagorinsky subgrid-scale modeling (Smagorinsky [6]; Germano et al. [7]; Lilly [8]) as follows:

$$\begin{aligned} &\frac{\partial v_i}{\partial t} + (v_j - w_j)\frac{\partial v_i}{\partial x_j} = \frac{1}{\rho}\frac{\partial}{\partial x_j}(\sigma_{ij} + \tau_{ij}^{SGS}) \qquad (i, j = 1,2,3) \qquad \text{in } \Omega^{\mathrm{f}} \\ &\frac{\partial v_i}{\partial x_i} = 0 \qquad (i = 1,2,3) \qquad \text{in } \Omega^{\mathrm{f}} \end{aligned} \tag{1}$$

In order to solve the flow problem, initial conditions on the flow variables v_i and p must be specified. In addition, appropriate boundary conditions must also be defined on $\Gamma_{\mathrm{t}}^{\mathrm{Tf}}$, which may be expressed as:

$$\begin{aligned} &v_i = w_i \qquad (i = 1,2,3) \qquad \text{on } \Gamma_{\mathrm{t}}^{\mathrm{fsi}} \qquad\qquad v_i = \overline{v}_i \qquad (i = 1,2,3) \qquad \text{on } \Gamma^{\mathrm{v}} \\ &p = \overline{p} \qquad \text{on } \Gamma^{\mathrm{p}} \qquad\qquad \sigma_{ij} n_j = \left[-p\delta_{ij} + \tau_{ij} \right] n_j = t_i = \overline{t}_i \qquad (i, j = 1,2,3) \qquad \text{on } \Gamma^{\sigma} \end{aligned} \tag{2}$$

where $\Gamma_{\mathrm{t}}^{\mathrm{fsi}}$ (boundary representing the fluid-structure interface), Γ^{v} (boundary with prescribed velocity $\overline{v}_i$), Γ^{p} (boundary with prescribed pressure $\overline{p}$) and Γ^{σ} (boundary with prescribed traction $\overline{t}_i$) are complementary subsets of $\Gamma_{\mathrm{t}}^{\mathrm{Tf}}$, such that $\Gamma_{\mathrm{t}}^{\mathrm{Tf}} = \Gamma_{\mathrm{t}}^{\mathrm{fsi}} \cup \Gamma^{\mathrm{v}} \cup \Gamma^{\mathrm{p}} \cup \Gamma^{\sigma}$. In Eq. (2), n_j are components of the unit normal vector **n** evaluated at a point on boundary Γ^{σ}. Notice that $w_i = 0$ is considered for points outside the ALE domain or when the immersed body is not moving.

2.2 PID control

A feedback control system is adopted here, where the input *u(t)* (control variable) is related to the angular orientation of the spoiler (actuator) with respect to the horizontal direction, while the output *y(t)* (process variable) is associated with the lift aerodynamic force resultant evaluated over the roof surface (sensor). A reference value for the process variable y_{sp} (setpoint) is defined initially, from which a control error e can be evaluated instantaneously over time, considering the difference between the reference value and the output ($e = y_{sp} - y$). Consequently, the control variable must be increased when the control error is positive and decreased otherwise.

A PID controller is defined as a superposition of three control components: proportional (P), integral (I) and derivative (I), which may be expressed as follows (Aström and Hägglund [3]):

$$u(t) = k_p \left(e_p(t) + \frac{1}{T_i}\int_0^t e(\tau)\, d\tau + T_D \frac{de_D(t)}{dt} \right) \tag{3}$$

where k_p is the proportional gain constant, while T_i and T_D are the integral and derivative times, respectively. The control errors are defined as:

$$e_p = by_{sp} - y \quad e_D = cy_{sp} - y \quad e = y_{sp} - y \tag{4}$$

where b and c are coefficients associated with load disturbances and noise measurements.

2.3 Numerical Model

The Characteristic-based Split (CBS) scheme is formulated considering a coordinate shift along the flow characteristic directions to remove the advective term from the flow fundamental equations, which permits the use of standard Galerkin procedures in finite element spatial discretizations without the emergence of numerical instabilities. Mesh updating is avoided by using Taylor series approximations in the spatial domain and a split operation is utilized following a numerical procedure proposed initially by Chorin [9] for incompressible flows in a finite difference context. The split operation enables the use of arbitrary interpolation functions for both the pressure and velocity fields and enhances pressure stability. Additional information on the CBS scheme may be found in Zienkiewicz et al. [10] and Nithiarasu et al. [11]. The standard Galerkin procedure is adopted here for spatial discretization of the flow equations after a temporal discretization operation is accomplished using the CBS scheme, where linear tetrahedral elements are utilized for both the velocity and pressure fields. Viscous and stabilizing terms are integrated by parts in steps 1 and 3, while the pressure Laplacian is integrated by parts in step 2, leading to boundary integral terms. A system of linear algebraic equations is then obtained for the discretized flow equations, which are expressed in matrix form as:

Step 1: intermediate velocity

$$\tilde{\mathbf{v}}_i = \mathbf{v}_i^n - \mathbf{M}_d^{-1}\Delta t\left[\left(\mathbf{A}+\mathbf{D}\right)\mathbf{v}_i - \frac{\Delta t}{2}\mathbf{S}_v - \mathbf{f}_i\right]^n \qquad (i=1,2,3) \tag{5}$$

Step 2: pressure calculation

$$\mathbf{H}\mathbf{p}^{n+1} = \frac{\rho}{\Delta t}\mathbf{G}_i^T\tilde{\mathbf{v}}_i \qquad (i=1,2,3) \tag{6}$$

Step 3: velocity correction

$$\mathbf{v}_i^{n+1} = \tilde{\mathbf{v}}_i - \mathbf{M}_d^{-1}\frac{\Delta t}{\rho}\left[\mathbf{G}_i\mathbf{p}^{n+1} + \frac{\Delta t}{2}\left(\mathbf{S}_p\right)_i\mathbf{p}^n\right] \qquad (i=1,2,3) \tag{7}$$

where $\mathbf{v}_i$ and $\mathbf{w}_i$ are the flow and mesh velocity vectors evaluated at nodal level, $\mathbf{p}$ is the pressure nodal vector and $\mathbf{M}_d$ is the discrete mass matrix, which is obtained from the consistent mass matrix $\mathbf{M}$.

The aerodynamic forces are locally evaluated considering any finite element sharing an element face with a fluid-structure interface, which may be expressed as:

$$\left(\mathbf{F}_i\right)_E = \int_{\Gamma_E}\mathbf{N}^T\left[\left(\mathbf{N}\bar{\mathbf{p}}\right)n_i - \left(\mu+\mu_t\right)\left(\frac{\partial\mathbf{N}}{\partial x_j}\bar{\mathbf{v}}_i\right)n_j\right]d\Gamma \qquad (i,\ j\ =\ 1,2,3) \tag{8}$$

where $\bar{\mathbf{v}}_i$ and $\bar{\mathbf{p}}$ are the flow velocity and pressure local vectors, while n_j are components of the unit normal vector $\mathbf{n}$ evaluated at a point on the interface. By using a typical finite element assembly procedure, aerodynamic force vectors $\mathbf{F}_I$ are then evaluated at nodal level.

A global time increment Δt is defined considering instantaneous flow conditions observed at element level, which leads to the following expression:

$$\Delta t = \min\left(\Delta t_{conv}, \Delta t_{dif}\right) \qquad \text{with} \qquad \Delta t_{conv} = \frac{l}{\|\mathbf{v}\|}; \qquad \Delta t_{dif} = \frac{l^2}{2Re} \tag{9}$$

where l is the finite element characteristic length, $\mathbf{v}$ is the vector of nodal velocities at element level and Re is the Reynolds number. A safety coefficient is applied to the global time increment obtained from Eq. (9), which usually ranges from 0.5 to 2 according to mesh characteristics and flow complexity.

The roof spoilers are considered here using the rigid body assumption. In the present model, spoilers can only rotate around the rotation axis at its trailing edge. In order to accommodate the spoiler motion within the flow spatial field, an ALE kinematic formulation and a mesh motion scheme are adopted. The flow problem on moving grids is adequately solved if the geometric conservation law (GCL) is satisfied (see Thomas and Lombard [12] for detailed information). According to Lesoinne and Farhat [13], the GCL is satisfied in ALE finite element formulations if the mesh velocity vector w is calculated as:

$$\mathbf{w} = \mathbf{v} = \frac{\mathbf{x}_{n+1} - \mathbf{x}_n}{\Delta t} \qquad \text{on } \Gamma_t^{\text{fsi}} \tag{10}$$

where $\mathbf{x}_n$ and $\mathbf{x}_{n+1}$ are nodal coordinate vectors referring to nodes belonging to moving fluid-structure interfaces, which are evaluated at time instants t_n and t_{n+1} within the time interval $\Delta t = t_{n+1} - t_n$.

3 Numerical examples

The numerical examples presented in this section were first analyzed by Loredo-Souza [14] using wind tunnel simulation. Figure 1 shows details about the computational domain utilized here, where boundary conditions, geometry of the building model and opening locations are indicated. Physical and numerical parameters used in the present simulations are presented in Table 1, which correspond to a flow with smooth and uniform conditions. Two-dimensional simulations are performed initially considering the building section cuts B-B and C-C, as illustrated in Fig. 1. These preliminary analyses are utilized to determine the validity of numerical predictions based on a two-dimensional approach using a LES-type model with adjustment of the Smagorinky's constant (the C-C section cut simulations intend to evaluate the circulation around and inside the building). In addition, simulations with the B-B section cut, refer to the evaluation of critical loads on the building roof where cases with and without opening are simulated considering the insertion of a fixed spoiler, as a manner to obtain the necessary parameters for the elaboration of the PID control theory and model calibration. Three-dimensional analyses complete the present investigation. The size of the smallest element is kept constant in regions around the body and wake, having a value equal to $3.0\text{x}10^{-4}L$, which leads to a dimensionless wall distance $y^+ = 4.10868$ for elements next to building surfaces, considering that $L = 1$ m. The location of measurement points for evaluation of internal and external pressures is based on positions utilized by Loredo-Souza [14].

Table 2 shows results related to force coefficients obtained over the building walls and the internal pressure coefficients for different wind incidences and building configurations, which are compared with experimental results presented by Loredo-Souza [14] and predictions indicated by the Brazilian standard NBR6123 (ABNT [15]). Notice that the test case galp04 leads to high positive pressures throughout the internal environment, producing overload conditions on the roof structure. The spoiler is hinged at the right end (edge) and rotation is allowed around the *y*-axis of the adopted coordinate system, varying between the counterclockwise and clockwise directions from the horizontal orientation (spoiler at 0°), with a maximum amplitude of ±12° (see Fig. 1).

Table 1. Physical and numerical parameters.

Parameter	Nomenclature	Value
Specific mass	ρ	1.2249 Kg/m³
Dynamic viscosity	μ	$3.8196\text{x}10^{-5}$ Ns/m²
Reference speed	V_∞	30.00 m/s
Reference dimension – building height	H	0.17825 m
Reynolds number	Re	1.4×10^5
Smagorisky's constant	Cs	0.1

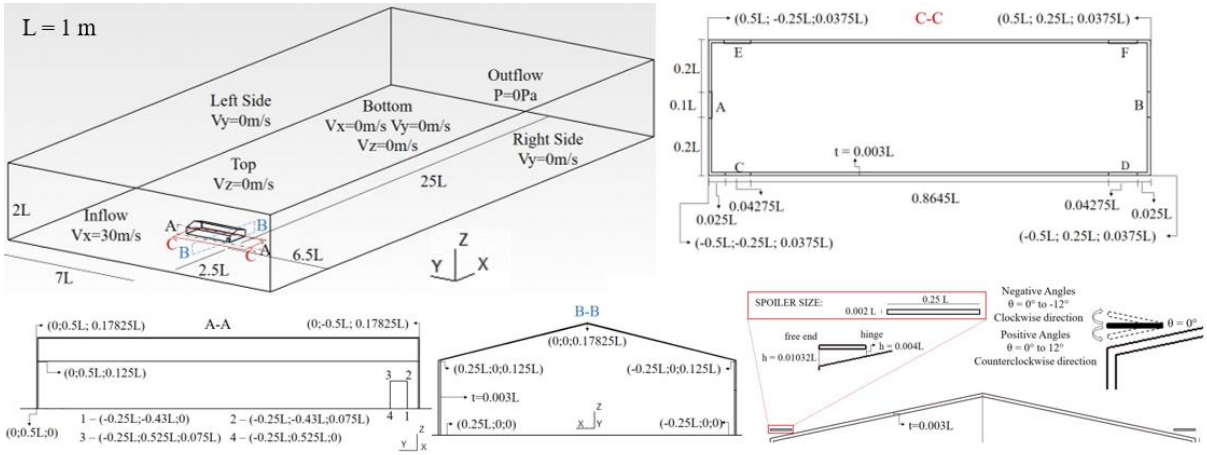

Figure 1. Computational domain, boundary conditions and geometric characteristics of the building model.

Table 2. Time-mean and r.m.s. force coefficients over the building walls and comparison of time-averaged internal pressure coefficients – C-C section cut.

Test case	Wind direction	Openings	Cx_m	Cx_{rms}	Cz_m	Cz_{rms}	100Ci [14]	100Ci [15]	100 Ci (present work)
galp01	90°	-	1.135	0.151	-0.049	0.262	-	-	-
galp02	0°	-	2.563	0.727	-1.015	2.692	-	-	-
galp03	0°	D	2.534	0.230	0.363	0.158	-	-	-
galp04	90°	A	-	-	-	-	50	80	51
galp05	90°	A, D and F	-	-	-	-	29	30	23
galp06	0°	A, D and F	-	-	-	-	-25	-20	-23

Simulations of a total of 28 test cases are performed and the corresponding results in terms of aerodynamic

coefficients and Strouhal number are presented in Table 3. The acronyms *sa* and *ca* utilized in Table 3 denote building configurations without and with opening, respectively, while *sa* and *sh* indicate the spoiler orientation in the counterclockwise and clockwise directions. The last two digits inform the spoiler orientation angle given in terms of degrees. According to the results presented in Table 3, one can see that the drag and uplift forces on the windward roof are significantly reduced for spoiler orientations within the clockwise rotation interval (negative angles). In this case, high suction peaks are minimized due to deviation of vortices from the roof surface, which were previously found very close to the roof. It is noteworthy that the presence of a spoiler with any orientation is sufficient to change considerably the pressure field and flow-induced forces on the roof. Instantaneous pressure fields obtained at t = 70 s are shown in Fig. 2 considering all the spoilers orientations analyzed in the present investigation, where building configurations with and without opening are utilized. One can see clearly that large vortices shed from the leading-edge of the roof are deviated upwards owing to the spoiler action.

Table 3. Time-averaged force coefficients: impermeable and permeable conditions

Spoiler angle	Test case	C_{zm} Windward	C_{xm} Windward	C_{zm} Leeward	*St* Spoiler	Teste Case	C_{zm} Windward	C_{xm} Windward	C_{zm} Leeward	*St* Spoiler
-	sa0000	2.534	-0.411	1.264	-	ca0000	3.049	-0.521	2.555	-
-12	sash12	1.274	-0.250	1.910	0.68	cash12	1.752	-0.356	2.314	0.56
-10	sash10	1.143	-0.225	1.785	0.55	cash10	1.721	-0.350	2.333	0.44
-8	sash08	1.033	-0.203	1.632	0.50	cash08	1.723	-0.351	2.308	0.38
-6	sash06	1.236	-0.243	1.794	0.45	cash06	1.710	-0.348	2.277	0.38
-4	sash04	1.348	-0.267	1.910	0.36	cash04	1.710	-0.349	2.344	0.32
-2	sash02	1.277	-0.254	1.787	0.24	cash02	1.763	-0.359	2.362	0.20
0	sash00	1.614	-0.351	1.722	0.11	cash00	1.953	-0.407	2.416	0.14
2	sasa02	1.597	-0.321	1.989	0.12	casa02	2.190	-0.452	2.456	0.11
4	sasa04	1.865	-0.377	1.739	0.10	casa04	2.629	-0.544	2.194	0.05
6	sasa06	2.129	-0.433	1.744	0.07	casa06	2.450	-0.500	2.243	0.06
8	sasa08	2.024	-0.408	1.719	0.04	casa08	2.436	-0.485	2.380	0.07
10	sasa10	2.082	-0.419	1.622	0.05	casa10	2.569	-0.527	2.260	0.04
12	sasa12	2.043	-0.414	1.703	0.05	casa12	2.516	-0.513	2.257	0.05

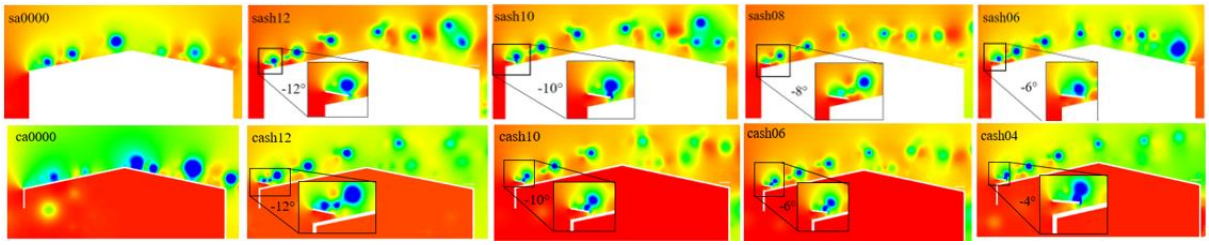

Figure 2. Instantaneous pressure fields for building configurations with and without opening.

The time-averaged force coefficient C_z and the distribution of time-averaged pressure over the upstream roof zone are the reference data used here to determine the PID control parameters, considering building configurations with and without opening. From the results obtained in the static analysis, one can elaborate the proportional gain curve k_p. The bandwidth (P_b) is obtained considering the maximum error amplitude and leads to a first approximation for the gain constant k_p. The spoiler is also submitted to dynamic analyses in order to obtain additional model parameters existing in the PID control equations. The dynamic analysis is performed here as follows: after the flow is fully developed at t = 40 s, the spoiler is allowed to rotate uniformly with angular velocity ω = -0,013963 rad/s, considering an initial orientation at 0° and increasing up to the optimal orientation angle. Notice that the angular velocity utilized for spoiler perturbation must be chosen carefully to avoid numerical instabilities. The PID control parameters obtained from the static and dynamic analyses are presented in Table 4.

Table 4. PID control parameters.

Parameter	Building without opening	Building with opening
Integral time (T_i)	50 seconds	25 seconds
Derivative time (T_D)	10 seconds	5 seconds
Dimensional coefficient (N)	8	8
Derivative Constant (c)	0.1	0.1
Sampling period (h)	1 second	1 second
Bandwidth (P_b)	1.096	0.912
Set point ($y_{sp} = Cz(\theta = \theta_{opt})$)	1.033 (θ_{opt} = -8°)	1.710 (θ_{opt} = -4°)
Gain constant (k_p)	0.382	0.456
Optimal angle – zero error (θ_{opt})	-8°	-4°

The three-dimensional analysis starts with the building models GP3D01 and GP3D02, which are investigated first to evaluate the distribution of external pressures on the building walls. The building models GP3D01 and GP3D02 correspond to the test cases galp01 and galp02 analyzed earlier. In the following analysis, a building model with an opening in the front wall (GP3D03) is also investigated (corresponding to the test case galp03). The test case GP3D04 is based on the geometric configuration utilized for the building model GP3D03, where spoilers with horizontal orientation are included near the windward and leeward roof edges. Table 5 shows results related to mean pressure and force coefficients evaluated on the roof of the building models analyzed in this work. Predictions obtained here with three-dimensional models are compared with results from similar building configurations using a two-dimensional approach (B-B section cut) and angle of wind incidence at 0°. In three-dimensional analysis, the motion of the windward spoiler is activated at t = 20 s using the PID control algorithm developed previously. A very stable process is obtained, where the optimal angle and optimal force coefficient values are achieved quickly, with the spoiler orientation oscillating within the angle interval [-4°, -6°]. Table 6 summarizes the results obtained here using two and three-dimensional models for a building configuration with opening and controlled spoiler.

Table 5. Time-averaged pressure and force coefficients on the building roofs for two and three-dimensional analysis.

Test cases	Windward roof			Leeward roof			Cp (ridge)
	Czm	Cxm	Cpm	Czm	Cxm	Cpm	
3D model, wind at 0° (GP3D02)	2.406	-0.405	-2.514	1.162	0.585	-1.131	-2.216
2D model, wind at 0° (sa0000)	2.534	-0.411	-2.706	1.264	0.503	-1.213	-2.219
3D model with opening, wind at 0° (GP3D03)	2.991	-0.579	-1.217	2.383	0.519	-1.114	-1.585
2D model with opening, wind at 0° (ca0000)	3.049	-0.521	-1.214	2.555	0.539	-1.177	-1.666
3D model with spoiler, wind at 0° (GP3D04)	1.931	-0.405	-1.022	2.412	0.396	-1.187	-1.109
2D model with spoiler, wind at 0° (cash00)	1.953	-0.407	-0.767	2.416	0.513	-1.148	-1.066

Table 6. Two and three-dimensional results for building configuration with opening and controlled spoiler.

Parameter	Two-dimensional analysis	Three-dimensional analysis
Optimal angle	-4°	-4° to -6°
C_{zm} (t < 20 s)	1.953	1.931
C_{zm} ($t \geq$ 20 s)	1.682	1.311
C_{xm} (t < 20 s)	-0.407	-0.405
C_{xm} ($t \geq$ 20 s)	-0.31	-0.28

4 Conclusions

A numerical investigation was proposed in this work to evaluate the influence of controlled spoilers on pressure mitigation over low-rise building roofs using PID control. A two-dimensional approach was initially adopted to verify the numerical formulation and computational meshes using the wind tunnel predictions referring to external pressure on building walls and internal pressure for building configurations with openings. A good agreement was observed between the experimental predictions and two-dimensional results obtained here. In addition, the control scheme was calibrated employing static and dynamic analyses based on a section cut of the three-dimensional

model, where spoilers were included along the windward and leeward roof edges. The control algorithm was formulated considering only wind-induced loads on the windward roof, since the pressure distribution on the leeward roof is not significantly altered by the spoiler orientation. From preliminary tests with a two-dimensional building it was observed that spoilers with clockwise orientation angles obtained significant reductions of aerodynamic loads on roof surfaces, by dissipating high pressure suctions at the roof ridge and windward edge, while deviating upwards the vortices shed from the spoiler. Optimal spoiler orientations of -8° and -4° were determined for building models without and with opening in the front wall. Building configurations with controlled spoilers were then simulated and results demonstrated that the control formulation proposed here was able to reduce the wind-induced loads on the building roofs to the desired limits. After the control mechanism is activated, the spoiler orientation changes slightly around the optimal angle, presenting angular displacements of small amplitude, while the aerodynamic forces on the roof show a very stable response over the time. Three-dimensional simulations were finally carried out and results compared with experimental predictions obtained from wind tunnel modeling and two-dimensional results obtained previously, where a good agreement was observed.

Acknowledgements. The authors would like to thank the National Council for Scientific and Technological Development (CNPq, Brazil) and the Brazilian Federal Agency for Support and Evaluation of Graduate Education (CAPES, Brazil) for the financial support. The present research was developed using computational resources provided by the High Performance Computing Center (NACAD/UFRJ, Brazil) and the National Center for High Performance Computing (CENAPAD/UNICAMP, Brazil).

Authorship statement. The authors hereby confirm that they are the sole liable persons responsible for the authorship of this work, and that all material that has been herein included as part of the present paper is either the property (and authorship) of the authors, or has the permission of the owners to be included here.

References

[1] G. Li, S. Gan, H. Li, Wind pressure mitigation on gable roofs for low-rise buildings using spoilers, Journal of Structural Engineering – ASCE 144(8) (2018) 1–14.
[2] L.A Sangalli, A.L. Braun, A fluid-structure interaction model for numerical simulation of bridge flutter using sectional models with active control devices. Preliminary results, Journal of Sound and Vibration 477 (2020) 1–33.
[3] K.J. Aström, T. Hägglund, PID Controllers, 2nd ed., Instrument Society of America, Research Triangle Park-NC 1995.
[4] K.J. Aström, T. Hägglund, Advanced PID Control, Instrument Society of America, Research Triangle Park-NC 2005.
[5] A.L. Braun, A.M. Awruch, Aerodynamic and aeroelastic analyses on the CAARC standard tall building model using numerical simulation, Computers and Structures 87(9-10) (2009) 564-581.
[6] J. Smagorinsky, General circulation experiments with the primitive equations, I, the basic experiment, Monthly Weather Review 91 (1963) 99-135.
[7] M. Germano, U. Piomelli, P. Moin, W.H. Cabot, A dynamic subgrid-scale eddy viscosity model, Physics of Fluids 3 (1991) 1760-1765.
[8] D.K. Lilly, A proposed modification of the Germano subgrid-scale closure method, Physics of Fluids 4 (1992) 633-635.
[9] A.J. Chorin, Numerical solution of Navier-Stokes equations, Mathematics of Computation 22 (1968) 745 –762.
[10] O.C. Zienkiewicz, R.L. Taylor, P. Nithiarasu, The Finite Element Method for Fluid Dynamics, 7th ed., Butterworth-Heinemann, Waltham, 2013.
[11] P. Nithiarasu, R.W. Lewis, K.N. Seetharamu, Fundamentals of the Finite Element Method for Heat and Mass Transfer, 2nd ed., Wiley, Chichester, West Sussex, 2016.
[12] P.D. Thomas, C.K. Lombard, Geometric conservation law and its application to flow computations on moving grids. AIAA Jl 17, 1030 (1979).
[13] M. Lesoinne, C. Farhat, Geometric conservation laws for flow problems with moving boundaries and deformable meshes, and their impact on aeroelastic computations, Computer Methods in Applied Mechanics and Engineering, 134(1-2) (1996) 71-90.
[14] A.M. Loredo-Souza. Influência do tipo de abertura e das características do vento simulado na pressão interna em um pavilhão industrial. Porto Alegre: UFRGS, 1992. Dissertação (Mestrado) – Programa de Pós-Graduação em Engenharia Civil, Universidade Federal do Rio Grande do Sul, Porto Alegre, 1992.
[15] ABNT, NBR6123 – Forças Devidas ao Vento em Edificações, Associação Brasileira de Normas Técnicas, Rio de Janeiro, 1988.